Autonomous Active Power Control for Islanded AC Microgrids with Photovoltaic Generation and Energy Storage System

Wu, Dan; Tang, Fen; Dragicevic, Tomislav; Vasquez, Juan Carlos; Guerrero, Josep M.

Published in:
I E E E Transactions on Energy Conversion

DOI (link to publication from Publisher):
10.1109/TEC.2014.2358612

Publication date:
2014

Document Version
Early version, also known as pre-print

Autonomous Active Power Control for Islanded AC Microgrids with Photovoltaic Generation and Energy Storage System

Dan Wu, Fen Tang, Tomislav Dragicevic, Juan C. Vasquez, Josep M. Guerrero

***Abstract*—In an islanded AC microgrid with distributed energy storage system (ESS), photovoltaic (PV) generation and loads, a coordinated active power regulation is required to ensure efficient utilization of renewable energy, while keeping the ESS from overcharge and over discharge conditions. In this paper, an autonomous active power control strategy is proposed for AC islanded microgrids in order to achieve power management in a decentralized manner. The proposed control algorithm is based on frequency bus-signaling of ESS and uses only local measurements for power distribution among microgrid elements. Moreover, this paper also presents a hierarchical control structure for AC microgrids that is able to integrate the ESS, PV systems and loads. Hereby, basic power management function is realized locally in primary level, while strict frequency regulation can be achieved by using additional secondary controller. Finally, real-time simulation results under various SoC and irradiance conditions are presented in order to prove the validity of proposed approach.**

***Index Terms*— Active power control, photovoltaic systems, energy storage system, secondary control, frequency bus-signaling.**

I. Introduction

A microgrid can be considered as a local grid with multiple distributed generators (DGs), energy storage system (ESS), and loads, able to operate either in grid-connected or islanded mode, with possibility of seamless transitions between them [1]. In islanded mode, the power exchange among DGs, ESS and loads should be balanced inside the isolated microgrid in order to keep the frequency stable.

Due to its installation cost decrease in recent years, photovoltaic (PV) generation has emerged as one of the major DG sources and is widely used in microgrids [2]-[4]. However, the intermittent nature of power supplied from the PV generation makes the ESS indispensable component to keep the power balance between generation and consumption. In islanded microgrid comprised of the ESS and PV generation, the ESS unit is usually operated as a grid forming unit that regulates AC bus, while the PV systems work as grid feeding units that inject all available power into the system [5]. In this sense, the ESS plays an important role for achieving the goal of power balance and grid frequency support in a safe range of state of charge (SoC). However, this simple active power regulation strategy will lead SoC out of safe region if imbalance between consumption and generation lasts long enough. These situations are referred to overcharge and over discharge condition, and it is well known that they may bring permanent damage to the ESS. On the other hand, strict active power regulation of the ESS to maintain it within the safe SoC limits while ignoring the imbalance of power generation and consumption will deteriorate the frequency regulation function [6]. Hence, the coordinated active power control strategy should take into account status of all microgrid elements such as the SoC of ESS, power available from the PV systems, and demand of power consumption.

At the same time, such a coordinated power control strategy needs to be designed with respect to specific microgrid configurations [7]. The most popular and well-known control paradigm in that sense is centralized control structure [8-10]. The multiple functions can be conveniently integrated into the microgrid central controller which collects measurement signals from all elements and sends back commands after processing the data through its own algorithm. Due to limited amount of data that it can process and inherent single point of failure, it is much more appropriate to implement this kind of controller in concentrated systems.

Decentralized control structure removes the central controller and the operation of system is regulated by a number of local controllers which can optionally communicate with one another [11], [12]. The limitation of physical location can be overcome, but communication network may get complicated when microgrid contains a lot of distributed units. Other available paradigms include a hybrid control structure which groups the microgrid elements into sub-decentralized systems [13]. It combines the advantages of both central and decentralized control structures, but has complex element composition and the functions of each central and local controllers are not clearly defined. Moreover, the coordinated power control in all aforementioned research works still relies

Dan Wu, Tomislav Dragicevic, Juan C. Vasquez, Josep M. Guerrero are with Department of Energy Technology, Aalborg University, 9220 Aalborg East, Denmark (e-mail: dwu@et.aau.dk; tdr@et.aau.dk, juq@et.aau.dk, joz@et.aau.dk).

Fen Tang is with National Active Distribution Network Technology Research Center (NANTEC), Beijing Jiaotong University, Haidian District, Beijing 100044, China (e-mail: ftang_nego@126.com).

on external physical digital communication links.

In order to enhance system reliability and expandability, and ensure its robustness against the failure of external communication system, autonomous power control strategy is needed. Droop control strategy, using frequency deviation of each unit to distribute active power, is widely accepted to fit into this requirement [14], [15]. However, the active power distribution is based on unified local control algorithm, which ignores the inherent power regulation difference between the ESS and the renewable energy sources. For example, the power generation of PV systems is usually based on current control mode (CCM) inner loop that follows maximum power point tracking (MPPT) algorithm, while the ESS is based on voltage control mode (VCM) inner loop aimed to regulate the bus voltage and frequency. Another promising approach is imposing higher order frequency waveforms on DC and AC power lines to pass coordination signals [16], [17]. The multiple resonant frequencies of these signals should be properly designed to avoid overlapping, and the coordinated signals may introduce noises into the distributed units. Bus-signaling method, by using different bus voltage/frequency thresholds to trigger mode-changing actions for the DGs and the ESS coordination is proposed in [18]-[20]. However, when the number of DGs increases, it becomes difficult to determine the bus voltage/frequency thresholds. Recently, an interesting active power control law based on modified droop method is presented in [21], which takes into account both SoC, and available power in the ESS and renewable energy sources, respectively. Nevertheless, the switching actions of droop curves may trigger stability problems induced by sudden bus frequency changes in microgrids.

In this paper, a decentralized autonomous active power control strategy which is compatible with a hierarchical control scheme is proposed for islanded AC microgrids formed by the distributed ESS, the PV systems, and loads. Based on the proposed bus-signaling method, the coordination performance of power regulation among microgrid elements is achieved in a decentralized manner. Moreover, an optional centralized secondary control is defined for executing restoration of bus frequency when/if the islanded microgrid is required to reconnect with utility grid. The proposed autonomous active power control has several key advantages: 1) it keeps the SoC of ESS in a safe range, while efficiently utilizing the renewable energy from the PV systems, 2) active power control principle is simple and independent from inner control loop design which can be easily implemented on top of conventional ESS and PV control systems without altering inner loop structure, 3) coordinated active power distribution relies on continuous and smooth frequency bus-signaling to avoid sudden bus frequency changes. The proposed autonomous control strategy is an extension of our previous work described in [22], while a more complete description of autonomous active power control in full range of SoC, and its implementation taking into account the ESS and PV system prime sources are addressed in this paper.

II. System Description

An exemplary multiple bus microgrid, shown in Fig. 1, consists of one ESS which acts as a grid forming unit, two PV

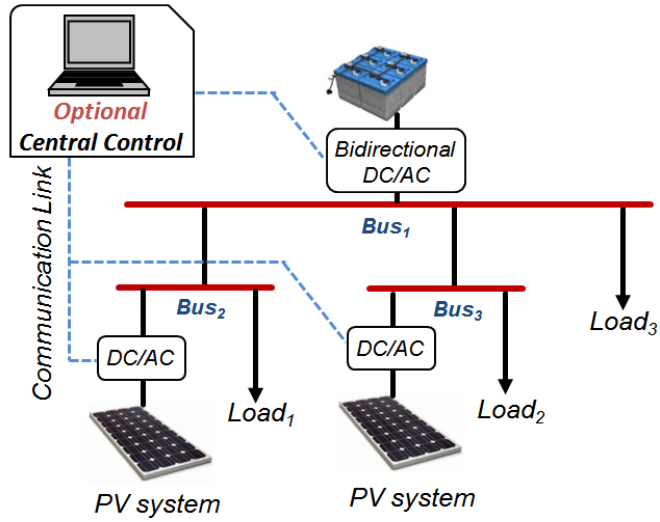

Fig. 1. An Islanded AC microgrid configuration with ESS and PV systems.

systems and distributed loads as grid following units. Battery bank system is used as the ESS which fixes bus frequency and compensates power imbalance between power generation and consumption. Each PV system is used to supply renewable energy to the microgrid.

A. ESS Grid Forming Unit.

Fig. 2 shows the configuration of the ESS unit, which consists of a battery bank, bidirectional converter and output filter. The modeling of the ESS with battery bank and associated SoC estimation algorithms are described in [23] in details. Based on Fig. 2, the grid forming unit control is implemented on grid connected DC/AC inverter, which is formed by a typical double loop VCM control and a grid frequency control (GFC). The inner loop VCM controller, using typical capacitor voltage controller (VC) and inductor current controller (CC), aims at fixing microgrid frequency and voltage. The frequency reference of inner loop is given by the GFC based on ESS condition, which is illustrated in Section III in details. The frequency-signaling performance is executed in the GFC by establishing a mapping between AC bus frequency and estimated SoC of battery. In this paper SoC is estimated with a simple ampere counting algorithm:

$$SoC(t) = SoC_0 + \int_0^t \eta_{bat} \cdot \frac{i_{bat}(t)}{C_{bat}} dt \qquad (1)$$

where SoC_0 is initial SoC, η_{bat} is charging/discharging efficiency, i_{bat} is battery current and C_{bat} is battery capacity. However, it should be noted that more advanced SoC algorithms may be directly used instead [24].

In this paper, only one ESS is used as a master unit. In cases when microgrid system needs to be upgraded to higher power ratings, multiple ESS units can be straightforwardly implemented by using ESS coordinated control, which is described in details in i.e. [25].

B. PV System Grid Following Unit.

Fig. 3 shows the configuration of the PV systems, which consists of the PV array, DC/AC converter, output filter and local control system. For detailed model construction of the

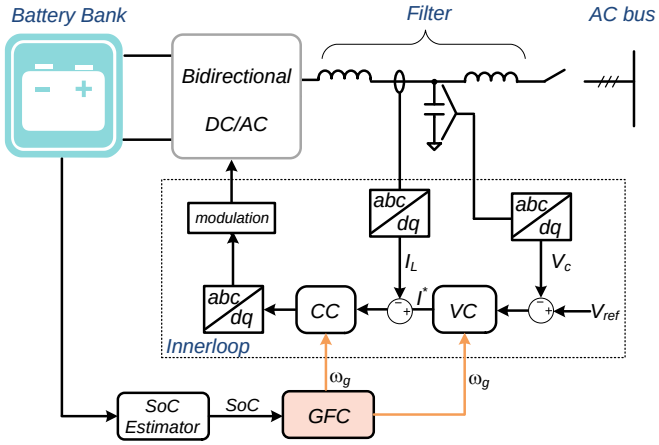

Fig. 2. ESS system configuration with power stage and control algorithm.

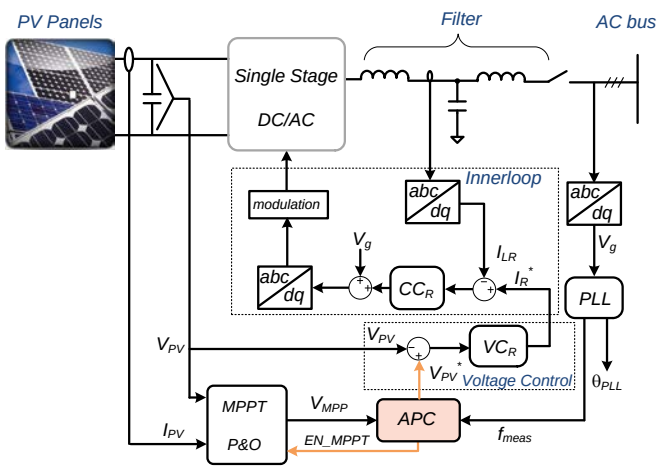

Fig. 3. PV system configuration with power stage and control algorithm.

PV panels, one may refer to [26]. In the control part, the output power generated by the PV system is regulated by the output voltage of PV panels V_{PV}, which operates at the MPP when the ESS has capability to compensate power imbalance. MPPT algorithm, shown in Fig. 3, utilizes perturb and observe method (P&O) [27], [28] to calculate the reference of V_{PV}. Then, three phase output currents are regulated by the typical CCM control structure including DC voltage controller VC_R and inner loop current controller CC_R which is implemented in *d-q* reference frame. An active power controller (APC) which is detailed in next section, is implemented to realize power curtailment when the PV system is required to decrease power generation and operate at off-MPP status. When executing power curtailment, the trigger signal EN_MPPT in Fig. 3 from the APC block is set to zero to disable the MPPT. Thereby the MPPT and power curtailment of the PV systems are never enabled at the same time.

III. Autonomous Active Power Control

The autonomous active power control and coordinated performance among microgrid components is achieved by frequency bus-signaling method throughout the microgrid system. This means that microgrid bus frequency is regulated by ESS master unit which uses frequency to reflect its SoC

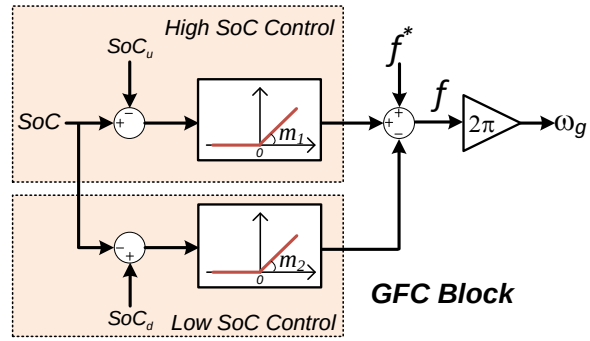

Fig. 4. GFC control algorithm of ESS.

condition, while the PV systems and distributed loads adjust power generation and consumption based on measured frequency.

A. ESS Master Control with GFC.

According to different SoC scenarios, the ESS bus-signaling control can be classified into high SoC control and low SoC control. The high SoC control targets the coordination between the ESS and PV system when microgrid system continuously generates excess of renewable energy which leads to high SoC level. When SoC becomes critically high and goes over the upper threshold SoC_u, the ESS boosts output frequency to inform the PV systems that they need to start decreasing power generation. In the high SoC range (SoC_u, 100%), shown as the GFC block in Fig. 4, the ESS regulates frequency with slope of m_1 for bus-signaling. Similarly, when SoC is below low-threshold SoC_d, the ESS is approaching over-discharge situation. In this range (SoC_0, SoC_d), the ESS controls bus frequency to constantly decrease from nominal value with slope m_2 to induce the loads shedding procedure. When the SoC is in the safe range (SoC_d, SoC_u), bus frequency is kept at nominal value f^*. The determination of SoC thresholds SoC_u and SoC_d takes into account the following issues: i) the higher SoC_u selected, the more efficiently can the renewable energy from PV system be used. ii) SoC has an estimation error and should give a margin of overcharge scenario (5% is considered in this paper). iii) Based on [29], SoC_d should be determined higher than the SoC value linked to end-voltage to protect the battery. Besides, the thresholds SoC_u and SoC_d are determined based on specific applications of battery systems, and a more detailed description of determining up and low SoC thresholds can be found in [30]. This bus-signaling control from ESS master unit can be expressed as

$$\begin{cases} f = f^* + m_1 \cdot (SoC - SoC_u) & SoC_u < SoC < 100\% \\ f = f^* & SoC_d \le SoC \le SoC_u \\ f = f^* - m_2 \cdot (SoC_d - SoC) & SoC_0 < SoC < SoC_d \end{cases} \quad (2a)$$

where the slopes m_1 and m_2 are determined as

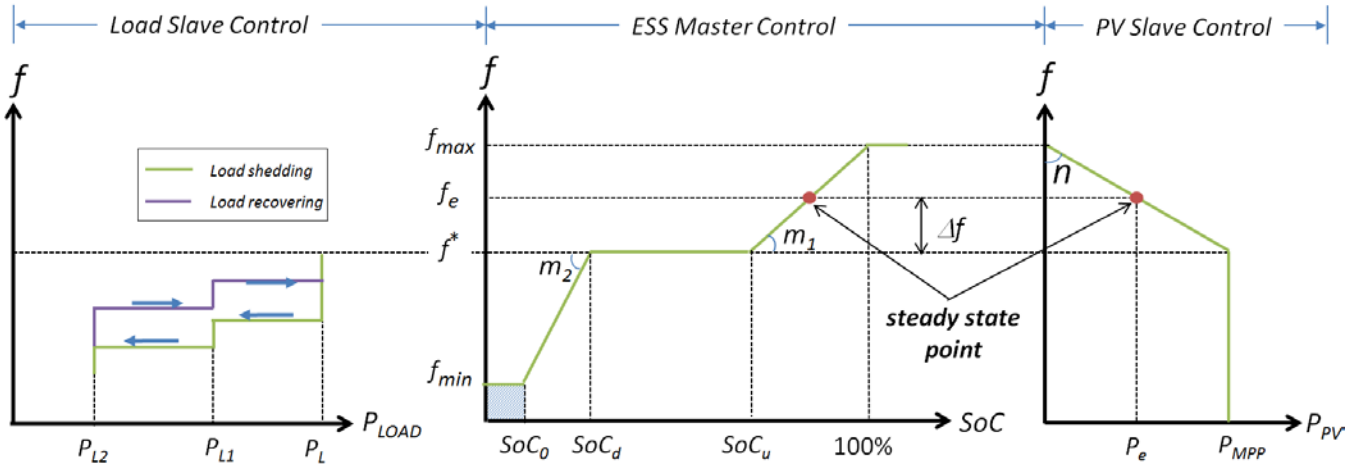

$$m_1 = \frac{f_{max} - f^*}{100\% - SoC_u} \tag{2b}$$

Fig. 5. Coordinated operation of microgrid based on master-slave control.

$$m_2 = \frac{f^* - f_{min}}{SoC_d - SoC_0} \tag{2c}$$

Finally, f_{max} and f_{min} represent maximum and minimum bus frequencies given by specific requirement of grid standard. When bus frequency reaches f_{min}, it indicates the SoC is below minimum threshold SoC_0 and there is not enough power stored to ensure normal system operation. At this time the overall system should be shut down. Fig. 5 shows this bus-signaling performance by the ESS. In addition, when bus frequency decays sharply due to failure scenarios of ESS master unit, microgrid can take actions: i) enabling VCM control mode in CCM units to perform grid support [20]; ii) connecting back-up equipment like diesel generators to support local loads. Multiple ESS can also be implemented in a coordinated way to improve system redundancy and avoid the single-point-failure of ESS master unit [25].

B. PV System Slave Control with APC.

Corresponding to different frequency ranges determined by the ESS, the PV systems adjust the output power depending on measured bus frequency f_{meas}. When f_{meas} is not above nominal frequency, PV systems are working at the MPP to make full use of renewable energy. When f_{meas} is above f^*, the PV systems start to decrease generated power to limit the SoC of the ESS reflected by frequency. In this way, the higher the bus frequency is, the lower power PV systems generate. This power regulation strategy can be expressed as

$$\begin{cases} P_{PV} = P_{MPP} & f_{meas} \le f^* \\ P_{PV} = P_{MPP} - n \cdot (f_{meas} - f^*) & f_{meas} > f^* \end{cases} \tag{3a}$$

$$n = \frac{P_{MPP}}{f_{max} - f^*} \tag{3b}$$

where P_{PV} is the output power of PV system, P_{MPP} is maximum power extracted from MPPT algorithm, and n is the slope of PV generation decrease with respect to frequency changes. Since MPPT algorithm is not enabled when $SoC > SoC_u$, the variable P_{MPP} in (3) in high SoC case refers to the last power status at MPP when SoC reached SoC_u, and is used as the initial point of active power control to decrease power

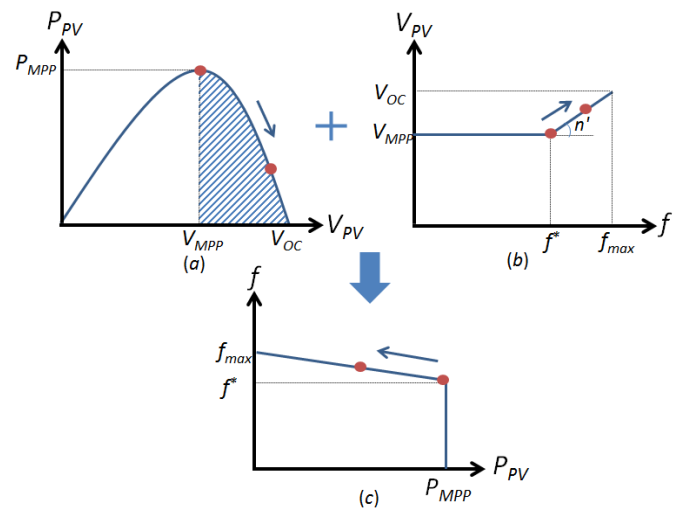

Fig. 6. PV system control with (a) V-P characteristic, (b) APC control and (c) inertia power control.

generation in order to have a smooth transition between two conditions.

Meanwhile, microgrid bus frequency f_{meas} is measured by the phase lock loop (PLL) block in PV systems. It can be expressed as,

$$f_{meas} = \frac{1}{\sigma s + 1} f \tag{3c}$$

where σ is time constant of bus frequency measurement for the APC control. When APC is enabled, taking (3c) into (3a) the output power of PV system can be deduced as,

$$P_{PV} = P_{MPP} - n\left(\frac{1}{\sigma s + 1} f - f^*\right). \tag{4}$$

By replacing f^* in (2a) when SoC $> SoC_u$ into (4), P_{PV} can be expressed as

$$P_{PV} = P_{MPP} + \frac{n\sigma s}{\sigma s + 1} f - n m_1 (SoC - SoC_u) \tag{5}$$

Based on (5) the partial derivative can be calculated as

$$\frac{\partial P_{PV}}{\partial f}=\frac{\Delta P_{PV}}{\Delta f}=\frac{n\sigma s}{\sigma s+1} \tag{6}$$

Then output power inertia of the PV systems can be deduced as [31]

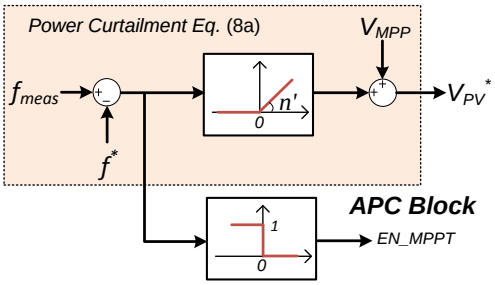

Fig. 7. APC control algorithm in the PV systems.

$$G_i(s)=\frac{\Delta P_{PV}}{s\Delta f}=\frac{n\sigma}{\sigma s+1} \tag{7}$$

Since n is fixed by (2b), the inertia response of the PV systems can be tuned independently of the time constant σ. Usually the time constant of PLL used in the CCM inner loop control is within 1s to ensure fast dynamic of current tracking. Compared to the time constant of inner loop PLL, the boost of bus frequency determined by the SoC, as presented in (2), is changing much slower (σ>>1s). Therefore, when designing the APC algorithm, the dynamics of inner loop control and active power regulation can be considered decoupled. The rate of frequency is much slower than inner power control loops. Thus the sensitivity of power regulation against frequency change is relatively low. The slave control of the PV system based on APC is presented in Fig. 5. This frequency signaling principle for power regulation of the PV systems can be found in [32] with its application in microgrid described in [33].

The above description of the APC gives the final power regulation of the PV system using frequency bus-signaling. While implementing the APC on the PV controller in specific, it is achieved by controlling the PV panel output voltage V_{PV}, with the full structure being shown in Fig. 6. Based on V-P characteristic (Fig.6(a)), the PV system can operate either at MPP or off-MPP by controlling V_{PV} in the range (V_{MPP}, V_{OC}) (Fig.6(b)), where V_{MPP} is the PV panel voltage corresponding to P_{MPP} which is calculated from the MPPT block, V_{OC} is open circuit voltage of PV panels. Then instead of using (3) to control output power, the APC control establishes relationship between bus frequency f and V_{PV} to indirectly control P_{PV} (Fig.6(c)). The implementation of the APC block in the PV systems is shown in Fig. 7 and is expressed as

$$\begin{cases} V_{PV}=V_{MPP} & f_{meas}\le f^* \\ V_{PV}=V_{MPP}+n'\cdot(f_{meas}-f^*) & f_{meas}>f^* \end{cases} \tag{8a}$$

Similar as (3b), the voltage boosting coefficient n' in (8a) is derived as

$$n'=\frac{V_{OC}-V_{MPP}}{f_{max}-f^*} \tag{8b}$$

In Fig. 7 the signal EN_MPPT setting to 1 and 0 represent the PV systems operate under the MPP and power curtailment conditions respectively. The V_{MPP} is therefore only being tracked when $SoC \le SoC_u$. When SoC is in high scenario the value V_{MPP} is selected as an initial PV voltage status to execute APC control in off-MPP condition.

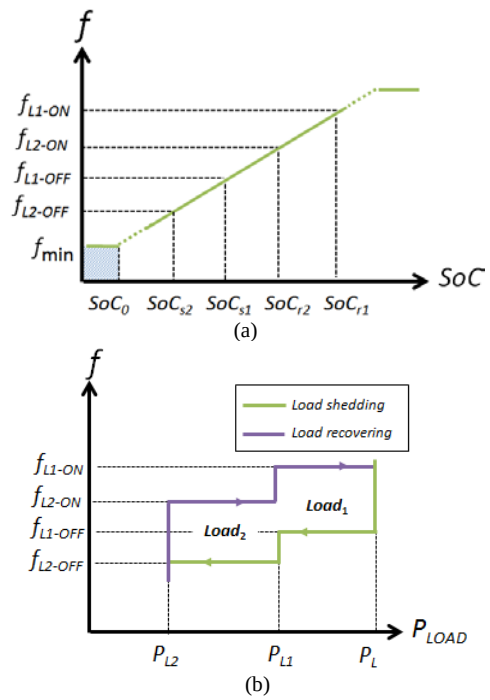

Fig. 8. Load slave control based on (a) frequency signling of ESS and (b) relay control of loads.

TABLE I
BUS-SIGNALING OF LOAD SLAVE CONTROL

Estimated SoC	Frequency thresholds	$Load_1$ status	$Load_2$ status
SoC_{r1}	f_{L1_ON}	ON	NC
SoC_{r2}	f_{L2_ON}	NC	ON
SoC_{s1}	f_{L1_OFF}	OFF	NC
SoC_{s2}	f_{L2_OFF}	NC	OFF

Note: NC indicates not changing action.

C. Load Slave Control.

Besides power generation, demand side management strategy in microgrid can also act as an effective energy reserve to meet supply-demand balance. According to different roles performed by microgrid loads, priorities are assigned to them. For example, critical devices are given as high priority, while non-critical loads that can be cut off when energy storage is low are assigned as low priority. Previous researches are proposed using frequency thresholds to perform loads shedding actions based on traditional droop control [34], [35]. These frequency thresholds are set corresponding to the load priorities. The loads with lower priorities are first cut off when frequency drops to preset levels. In this way the lower the bus frequency is, the loads with higher priority are shed one by one. The loads recovery process adopts similar manner, where loads with higher priorities are firstly recovered when bus frequency gets restored from lower to higher levels. This

principle of AC bus frequency signaling to perform loads shedding and recovery procedure is employed in this paper. However, the main difference is that the frequency signaling here is determined as a function of the SoC in (2a) but not instantaneous power, as presented in load slave control of Fig.

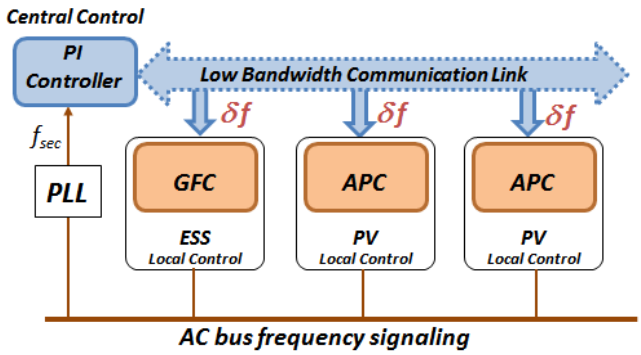

Fig. 9. Central secondary control configuration.

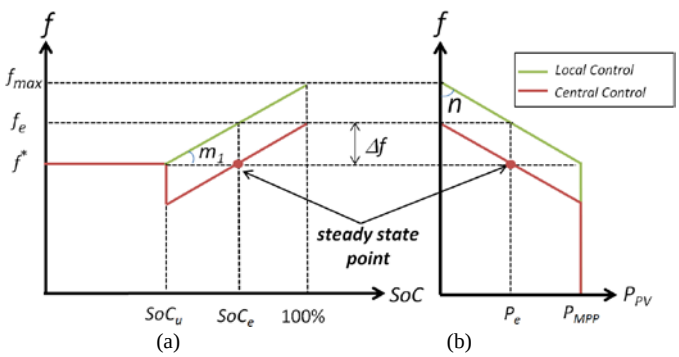

Fig. 10. Central secondary control performance. (a) ESS master control and (b) PV system slave control.

5. In this way, bus frequency triggers the on/off actions of load contactors depending on the SoC value of the ESS. Fig. 8(a) shows a two-step loads shedding procedure with bus-signaling, where $Load_2$ holds higher priority than $Load_1$. SoC_{r1}, SoC_{r2}, SoC_{s1}, SoC_{s2} represent SoC thresholds for connecting and tripping $Load_1$ and $Load_2$. And f_{L1_ON}, f_{L2_ON}, f_{L1_OFF} and f_{L2_OFF} represent frequency thresholds to close and open loads contactors. In order to avoid chattering phenomenon (repetitive ON-OFF actions of load contactors), a relay control is utilized, as shown in Fig. 8(b). The description of $Load_1$ and $Load_2$ status according to bus-signaling effect is summarized as Table I.

IV. Centralized Secondary Control

With only local autonomous active power control, steady state bus frequency deviation Δf will be produced as P_{PV} decreases to steady state point P_e, as shown in Fig. 5. Although maximum frequency deviation of Δf can be designed to stay within the preselected allowable range according to (1), it can also be completely eliminated by additional centralized secondary control when tight bus frequency regulation is required, as shown in Fig. 9. Notice that the communication link between the central and local level is of low bandwidth, and operates as an optional component since the coordination performance is already achieved by local power controller. This tradeoff between the investment in the communication link and high quality of power supply can be decided by customer with respect to requirements of different applications.

Fig. 10 shows the centralized secondary control performance for bus frequency restoration. When $SoC>SoC_u$,

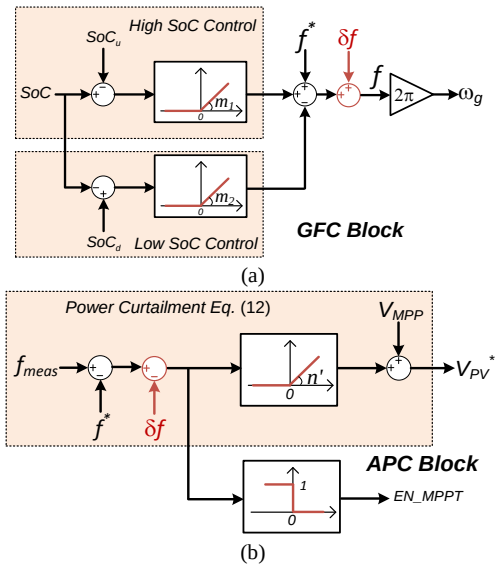

Fig. 11. Secondary control algorithm of (a) GFC block and (b)APC block.

TABLE II
POWER STAGE AND CONTROL PARAMETERS

Parameter	Symbol	Value	Unit
Power Stage			
Nominal Bus Voltage	V^*	230	V
Nominal Bus Frequency	f^*	50	Hz
Inverter Inductor of ESS	L_{in}	1.8	mH
Output Inductor of ESS	L_o	1.5	mH
Filter Capacitor	C	27	μF
Output Inductor of PV	L_f	3.6	mH
Active Power Loads	$R_1/R_2/R_3$	300	Ω,
Reactive Power Loads	$L_1/L_2/L_3$	0.4/0.4/0.5	H
Inner loop Control			
ESS Voltage Controller	k_{pV}, k_{iV}	0.1, 200	-, s^{-1}
ESS Current Controller	k_{pI}, k_{iI}	15,50	-, s^{-1}
PV Current Controller	k_{pPV}, k_{iPV}	20,50	-, s^{-1}
Active Power Control			
Maximum Bus Frequency	f_{max}	50.5	Hz
SoC Upper-threshold	SoC_u	95	%
SoC Low-threshold	SoC_d	40	%
Boosting Slope of Frequency	m_1	0.1	Hz/%
Dropping Slope of Frequency	m_2	0.4	Hz/%
Tripping Thresholds of Loads	$f_{L1\text{-}OFF}$, $f_{L2\text{-}OFF}$,	49.5 49.4	Hz
Recovery Thresholds of Loads	$f_{L1\text{-}ON}$, $f_{L2\text{-}ON}$	49.8 49.7	Hz

both response of the ESS master control and the PV system slave control shift downward by the restoration term δf sent from central controller. The central secondary control monitors

the AC bus frequency and utilizes PI controller for the bus frequency restoration that can be expressed as

$$\delta f = G_s(s)\cdot(f^* - f_{sec}) = \left(k_{psec} + \frac{k_{isec}}{s}\right)\cdot(f^* - f_{sec}) \qquad (9)$$

where $G_s(s)$ is the central secondary controller with k_{psec} and k_{isec} as proportional and integral terms, and f_{sec} is measured bus frequency by the central controller.

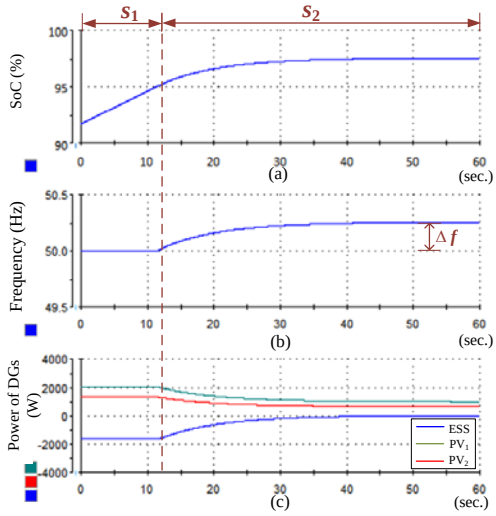

Fig. 12. Simulation results in high SoC scenario of ESS with only local active power control.

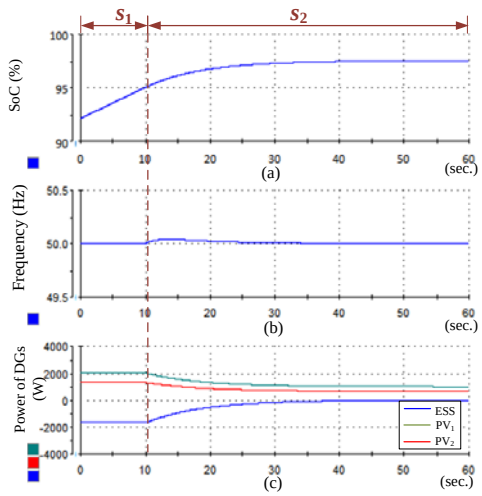

Fig. 13. Simulation results in high SoC scenario of ESS with both local and central control.

With restoration term δf, the ESS and the PV system coordination response based on (2) and (3) can be rewritten as

$$f = f^* + \delta f + m_1\cdot(SoC - SoC_u) \qquad SoC_u < SoC < 100\% \quad (10)$$

$$P_{PV} = P_{MPP} - n\cdot(f_{meas} - f^* - \delta f) \qquad f_{meas} > f^* + \delta f \qquad (11)$$

Corresponding to (11), the APC control strategy of the PV system is revised as

$$V_{PV} = V_{MPP} + n'\cdot(f_{meas} - f^* - \delta f) \qquad f_{meas} > f^* + \delta f \qquad (12)$$

Based on (10) and (12), the control blocks of the GFC and APC with secondary control are shown in Fig. 11. By combining (9)-(11), it can be deduced that the inertia response of the PV system is consistent with (7), which indicates that the effect of secondary frequency restoration is decoupled from the local active power regulation.

V. Hardware-in-the-loop Results

The proposed autonomous active power control strategy is implemented on an islanded AC microgrid consists of one ESS, two PV systems and three distributed load, as shown in Fig. 1. The power stage and control parameters are presented

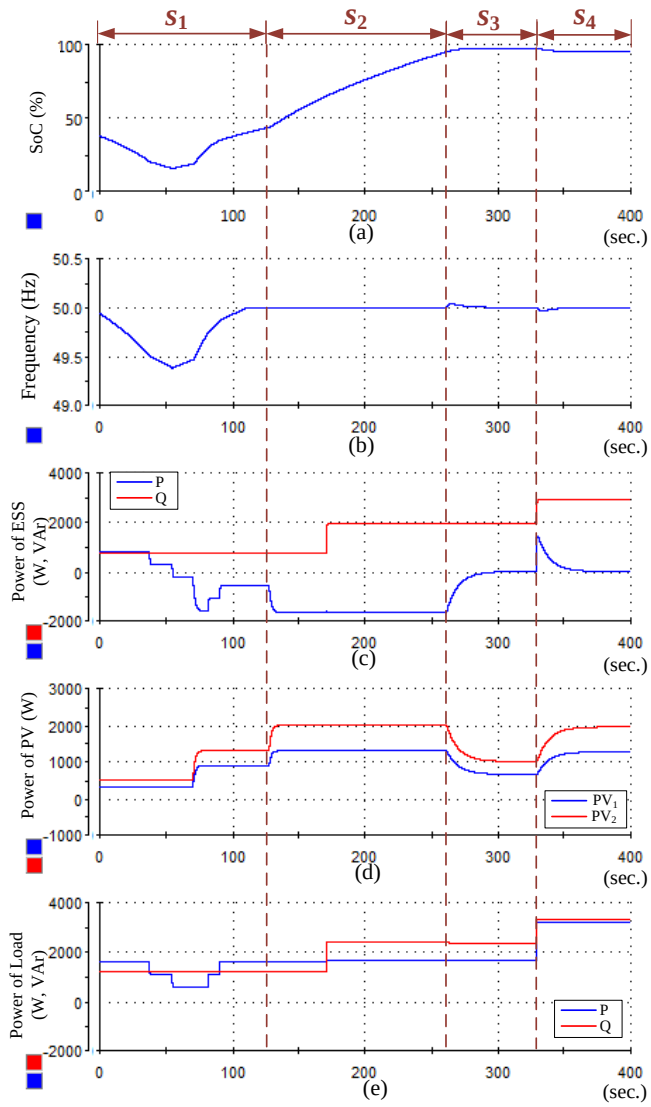

Fig. 14. Simulation results in full SoC scenario of coordination with ESS, PV systems and distributed loads.

in Table II. The overall microgrid model is established with MATLAB/Simulink toolbox and then downloaded into dSPACE 1006 platform based on real-time simulation, in which the time span of simulation equals to that in the real system. Fig. 12 shows simulation results with local active power control between the ESS and PV system which is summarized as

- Scenario S_1: The SoC of the ESS (Fig. 12(a)) is lower than the 95%, so that two PV systems are operating at 2kW and 1.3kW respectively. And ESS is charging power of 1.72kW (Fig. 12(c)). Bus frequency is kept at nominal value 50Hz (Fig. 12(b)).

- Scenario S_2: The SoC of ESS is above 95%, and bus frequency is increasing to inform power decrease from PV systems. Both PV systems receive that frequency and gradually decrease their generation to 0.95kW and 0.62kW, respectively. In this way the charging power gets limited to zero with time. In steady state, the bus frequency is stable at 50.3Hz.

Fig. 13 shows the simulation results with both local and central control for active power regulation. Compared with Fig. 12, it can be seen that coordination performance of active power regulation (Fig. 13(c)) remains the same with only local control shown in Fig. 12. However, with central control, the bus frequency deviation can be effectively eliminated in steady state (Fig. 13(b)).

Fig. 14 shows simulation results of coordinated performance of the ESS, the PV systems and distributed loads

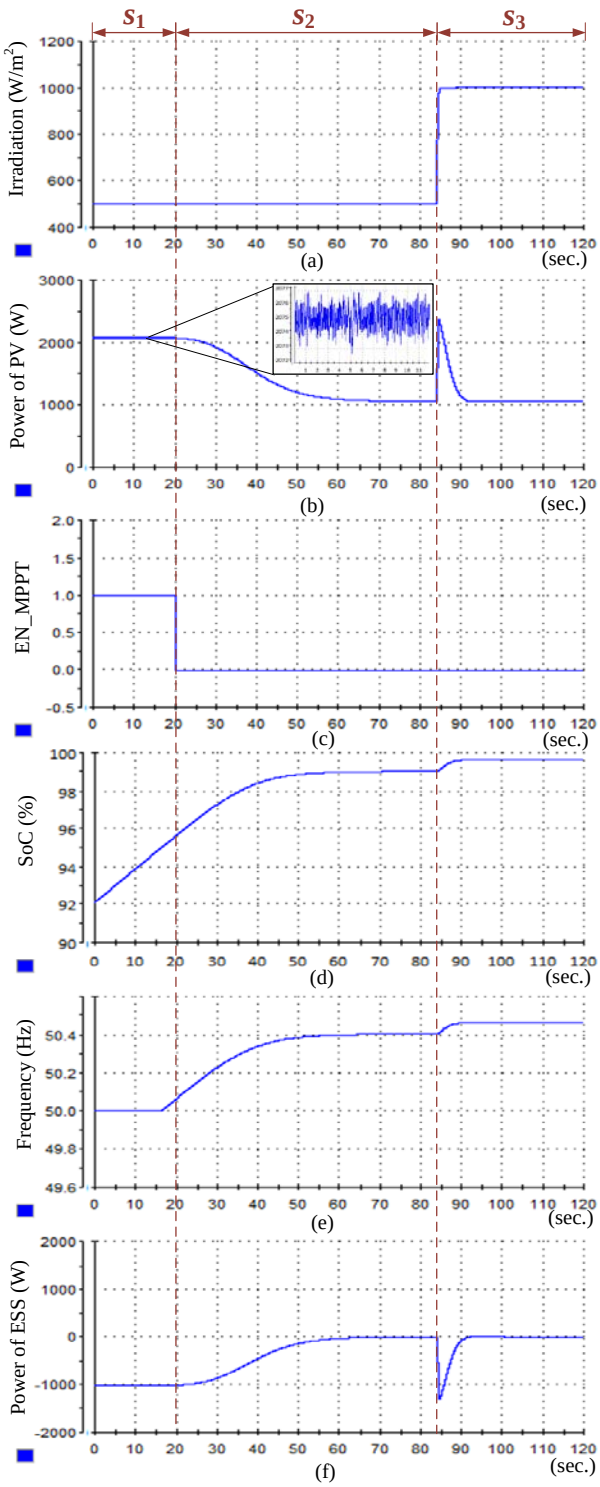

Fig. 15. Simulation results of system performance when 50% solar irradiation increases from 500 to 1000 W/m^2.

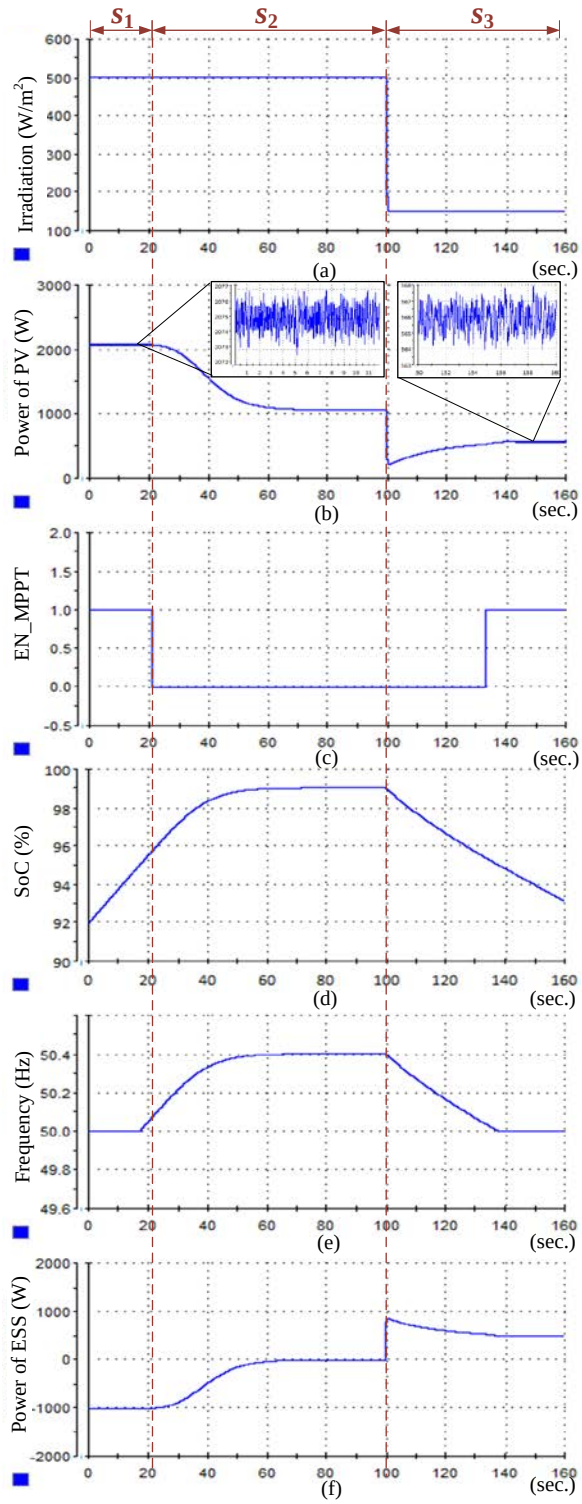

Fig. 16. Simulation results of system performance when 70% solar irradiation decreases from 500 to 150 W/m^2.

in full range of SoC, which is summarized as

- Scenario S_1: The SoC is in low range that there is coordination with ESS and distributed loads. When SoC drops to 20% and 15%, two parts of non-critical load are successively tripped by measuring the bus frequency drops to 49.5Hz and 49.4Hz. When the SoC rises up to 30% and 35% at 49.7Hz and 49.8Hz respectively, the two parts of loads are recovered successively.

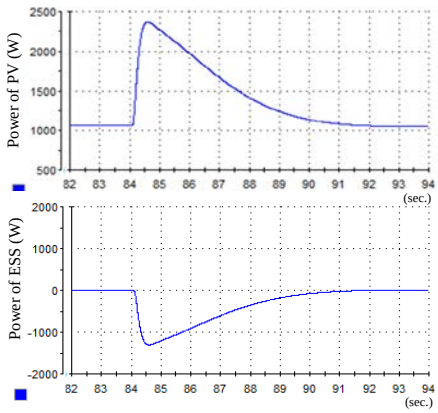

Fig. 17. Simulation results of system dynamic performances when solar irradiation suddenly increases.

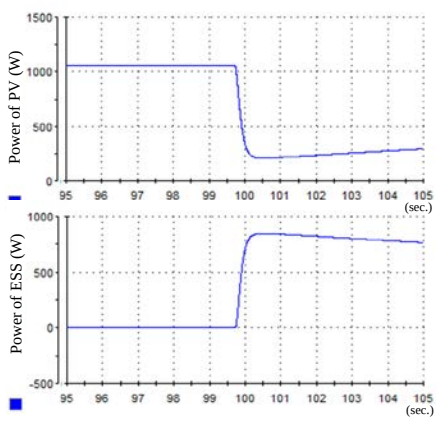

Fig. 18. Simulation results of system dynamic performances when solar irradiation suddenly drops.

- Scenario S_2: The SoC is in moderate range, then the PV generation are 2kW and 1.3kW. The bus frequency is controlled at 50Hz in this range. In this scenario, reactive power changes from 1.2kVAr to 2.4kVAr with power factor changing from 0.8 to 0.5, and the overall microgrid system maintains good dynamic performance.
- Scenario S_3: The microgrid operation is based on coordination between the ESS and PV systems to limit the ESS charging power by decreasing power generation in high SoC case, similarly shown in Fig. 13.
- Scenario S_4: Total active power load increases 3.2kW, while reactive power load increases to 3.4kVAr. It can be seen that the instantaneous increased active and reactive power is generated by the ESS. Afterward, the PV systems gradually restore generation again in an autonomous way. It can be seen after a short dynamic process that the bus frequency is regulated at 50Hz in steady state. Same as shown in S_2, the autonomous power regulation performance can be maintained and a sudden reactive power changes have little effect.

Fig. 15 shows simulation results of microgrid system performance when sudden solar irradiation increases from 500 to 1000 W/m^2,

- Scenario S_1: The ESS is in the moderate SoC condition (Fig. 15(d)), while irradiation of Fig. 15(a) is 500 W/m^2. In this range, the PV system operates at MPP with 2075 W (see Fig. 15(b)) by using MPPT algorithm (enable MPPT signal is set at unity in Fig. 15(c)). The dynamic of MPP tracking is shown in Fig. 15(b).
- Scenario S_2: The ESS is approaching to be fully charged (SoC is above 95% in Fig. 15(d)), and the APC control dominates the PV system to gradually decrease power generation (Fig. 15(b)). In this range, the MPPT algorithm is stalled, as Fig. 15(c) shows. In order to show frequency behavior followed by coordination between ESS and PV system, secondary control is not presented here (see Fig. 15(e)). Also, it can be noticed that when the APC control is enabled, a dead band is set at 0.05Hz around the nominal bus frequency 50Hz to decrease sensitiveness of instantaneous frequency ripple.
- Scenario S_3: Solar irradiation changes from 500 to 1000 W/m^2. The PV system tends to generate higher power of 2375W due to increased solar irradiation. This instantaneous generated power from the PV system can be absorbed by ESS at 1250W in Fig. 15(f). Then resulting from the APC control, the PV generation is able to decrease power again to limit charging power of the ESS (Fig. 15(b) and Fig. 15(f)).

Fig. 16 shows simulation results of overall microgrid system performance when sudden solar irradiation decreases from 500 to 150 W/m^2 to simulate partial shading situation,

- Scenarios S_1 and S_2: Solar irradiation is 500 W/m^2, and microgrid system performance can be referred to scenarios S_1 and S_2 of Fig. 15.
- Scenarios S_3: 70% solar irradiation changes from 500 W/m^2 to 150 W/m^2, in case of partial shading. The instantaneous power generation decrease is supported by the ESS (Fig. 16(f)). Then SoC of ESS starts to decrease as ESS discharges power to supply power together with PV system (Fig. 16(d)). Corresponding to the SoC decrease, the microgrid bus frequency also decreases by bus signaling effect (Fig. 16(e)). When the SoC drops to threshold SoC_u=95%, MPPT algorithm is enabled again (Fig. 16(c)) and the PV system operates at MPP of 576W (Fig. 16(b)). The dynamics of MPP tracking of the PV generation in S_1 and S_3 are shown in Fig. 16(b).

Fig. 17 shows the dynamics of the PV and ESS systems when solar irradiation increases, as presented in Fig. 15. Although the PV system generates higher power at 2475 W instantaneously, the power generation can be suppressed in short time due to APC control to limit ESS charging power.

Fig. 18 shows dynamics of the PV and ESS systems when solar irradiation decreases suddenly as presented in Fig. 16. In the dynamic process, the sudden power generation drop is

supported by ESS system, while PV system gradually restores power generation to supply loads together with the ESS.

VI. Conclusion

This paper proposed an autonomous active power control to coordinate distributed components of microgrid consisting of the ESS, the PV systems and loads. Additionally, a centralized secondary control was applied to effectively eliminate steady state deviation of the bus frequency. By the proposed active power control, SoC of the ESS can be kept within the safe limits by automatically adjusting the power generation from the PV systems and load consumption. This coordination performance was obtained by using only local controllers and does not rely on external communication links. Therefore, the risk induced by the failure of the communication links can be avoided and thereby the reliability of the system is enhanced. Finally, the proposed control strategy is verified by the hardware-in-the-loop simulation results.

References

[1] J. M. Guerrero, M. Chandorkar, T. Lee, P. C. Loh, "Advanced Control Architectures for Intelligent Microgrids—Part I: Decentralized and Hierarchical Control," *IEEE Trans. Ind. Electron*, vol.60, no.4, pp.1254-1262, April 2013.

[2] M. Datta, T. Senjyu, A. Yona, T. Funabashi, Kim Chul-Hwan, "A Frequency-Control Approach by Photovoltaic Generator in a PV–Diesel Hybrid Power System," *IEEE Trans. Energy Conv.*, vol.26, no.2, pp.559-571, June 2011.

[3] S. B. Kjaer, J. K. Pedersen, and F. Blaabjerg, "A review of single-phase grid-connected inverters for photovoltaic modules," *IEEE Trans. Ind. Appl.*, vol. 41, no. 5, pp. 1292–1306, Sep./Oct. 2005.

[4] Q. Li and P. Wolfs, "A review of the single phase photovoltaic moduleintegrated converter topologies with three different DC link configurations," *IEEE Trans. Power Electron.*, vol. 23, no. 3, pp. 1320–1333, May 2008.

[5] L. J. Ricalde, E. Ordonez, M. Gamez, and E. N. Sanchez, "Design of a smart grid management system with renewable energy generation," in *2011 IEEE Symposium on Computational Intelligence Applications In Smart Grid (CIASG)*, 2011, pp. 1–4.

[6] F. Giraud, Z. M. Salameh, "Steady-state performance of a grid-connected rooftop hybrid wind-photovoltaic power system with battery storage," in *IEEE Power Engineering Society Winter Meeting.* , 2001, vol. 3, p. 978.

[7] H. Nehrir, K. Strunz, H. Aki, J. Bing, and Z. Salameh, "A review of hybrid renewable/alternative energy systems for electric power generation: Configurations, control and applications," in *2012 IEEE Power and Energy Society General Meeting*, 2012, pp. 1–1.

[8] K. Jong-Yul, J. Jin-Hong, K. Seul-Ki, C. Changhee, P. June-Ho; K. Hak-Man, N. Kee-Young, "Cooperative Control Strategy of Energy Storage System and Microsources for Stabilizing the Microgrid during Islanded Operation," *IEEE Trans. Power Electron*., vol.25, no.12, pp.3037,3048, Dec. 2010.

[9] H. Kanchev, L. Di, F. Colas, V. Lazarov, B. Francois, "Energy Management and Operational Planning of a Microgrid With a PV-Based Active Generator for Smart Grid Applications," *IEEE Trans. Ind. Electron*, vol.58, no.10, pp.4583-4592, Oct. 2011.

[10] F. Valenciaga and P. F. Puleston, "Supervisor Control for a Stand-Alone Hybrid Generation System Using Wind and Photovoltaic Energy," *IEEE Trans. Energy Convers.*, vol. 20, no. 2, pp. 398–405, Jun. 2005.

[11] A. L. Dimeas and N. D. Hatziargyriou, "Operation of a Multiagent System for Microgrid Control," *IEEE Trans. Power Syst.*, vol. 20, no. 3, pp. 1447–1455, Aug. 2005.

[12] J. Lagorse, M. G. Simoes, and A. Miraoui, "A Multiagent Fuzzy-Logic-Based Energy Management of Hybrid Systems," *IEEE Trans. Ind. Appl.*, vol. 45, no. 6, pp. 2123–2129, 2009.

[13] M. S. Khan and M. R. Iravani, "Supervisory Hybrid Control of a Micro Grid System," in *2007 IEEE Canada Electrical Power Conference*, 2007, pp. 20–24.

[14] Dan Wu; Fen Tang; Guerrero, J.M.; Vasquez, J.C.; Guoliang Chen; Libing Sun, "Autonomous active and reactive power distribution strategy in islanded microgrids," in *2014 Applied Power Electronics Conference and Exposition (APEC)*, pp.2126-2131, March 2014.

[15] E. A. A. Coelho, P. C. Cortizo, and P. F. D. Garcia, "Small-signal stability for parallel-connected inverters in stand-alone AC supply systems," *IEEE Trans. Ind. Appl.*, vol. 38, no. 2, pp. 533–542, 2002.

[16] T. Dragicevic, J. M. Guerrero, and J. C. Vasquez, "A Distributed Control Strategy for Coordination of an Autonomous LVDC Microgrid Based on Power-Line Signaling," *IEEE Trans. Ind. Electron.*, vol. 61, no. 7, pp. 3313–3326, Jul. 2014.

[17] D. J. Perreault, R. L. Selders, and J. G. Kassakian, "Frequency-based current-sharing techniques for paralleled power converters," *IEEE Trans. Power Electron.*, vol. 13, no. 4, pp. 626–634, Jul. 1998.

[18] D. Boroyevich, I. Cvetkovic, D. Dong, R. Burgos, F. Wang, and F. Lee, "Future electronic power distribution systems a contemplative view," in *Proc. Int. Optimization of Electrical and Electronic Equipment Conf.*, 2010, pp. 1369–1380.

[19] J. Schonberger, R. Duke, and S. D. Round, "DC-Bus Signaling: A Distributed Control Strategy for a Hybrid Renewable Nanogrid," *IEEE Trans. Ind. Electron.*, vol. 53, no. 5, pp. 1453–1460, Oct. 2006.

[20] D. Wu, J. M. Guerrero, J. C. Vasquez, T. Dragicevic, and F. Tang, "Coordinated power control strategy based on primary-frequency-signaling for islanded microgrids," in *2013 IEEE Energy Conversion Congress and Exposition*, 2013, pp. 1033–1038.

[21] J. G. de Matos, L. A. de S. Ribeiro, and E. de Carvalho Gomes, "Power control in AC autonomous and isolated microgrids with renewable energy sources and energy storage systems," in *IECON 2013 - 39th Annual Conference of the IEEE Industrial Electronics Society*, 2013, pp. 1827–1832.

[22] D. Wu, F. Tang, T. Dragicevic, J. C. Vasquez, and J. M. Guerrero, "Coordinated primary and secondary control with frequency-bus-signaling for distributed generation and storage in islanded microgrids," in *IECON 2013 - 39th Annual Conference of the IEEE Industrial Electronics Society*, 2013, pp. 7140–7145.

[23] T. Dragicevic, J. M. Guerrero, J. C. Vasquez, and D. Skrlec, "Supervisory Control of an Adaptive-Droop Regulated DC Microgrid With Battery Management Capability," *IEEE Trans. Power Electron.*, vol. 29, no. 2, pp. 695–706, Feb. 2014.

[24] T. Dragicevic, S. Sucic, and J. M. Guerrero, "Battery state-of-charge and parameter estimation algorithm based on Kalman filter," in *Eurocon 2013*, 2013, pp. 1519–1525.

[25] X. Lu, K. Sun, J. M. Guerrero, J. C. Vasquez, and L. Huang, "State-of-Charge Balance Using Adaptive Droop Control for Distributed Energy Storage Systems in DC Microgrid Applications," *IEEE Trans. Ind. Electron.*, vol. 61, no. 6, pp. 2804–2815, Jun. 2014.

[26] M. G. Villalva, J. R. Gazoli, and E. R. Filho, "Comprehensive Approach to Modeling and Simulation of Photovoltaic Arrays," *IEEE Trans. Power Electron.*, vol. 24, no. 5, pp. 1198–1208, May 2009.

[27] R. A. Mastromauro, M. Liserre, and A. Dell'Aquila, "Control Issues in Single-Stage Photovoltaic Systems: MPPT, Current and Voltage Control," *IEEE Trans. Ind. Informatics*, vol. 8, no. 2, pp. 241–254, May 2012.

[28] T. Esram and P. L. Chapman, "Comparison of Photovoltaic Array Maximum Power Point Tracking Techniques," *IEEE Trans. Energy Convers.*, vol. 22, no. 2, pp. 439–449, Jun. 2007.

[29] D. Linden and T. B. Reddy, *Handbook of batteries*. McGraw-Hill, 2002.

[30] B. Xiao, Y. Shi, and L. He, "A universal state-of-charge algorithm for batteries," *Design Automation Conference (DAC), 2010 47th ACM/IEEE* , vol., no., pp.687,692, 13-18 June 2010.

[31] M. Datta, H. Ishikawa, H. Naitoh, and T. Senjyu, "LFC by coordinated virtual inertia mimicking and PEVs in power utility with MW-class distributed PV generation," in *2012 IEEE 13th Workshop on Control and Modeling for Power Electronics (COMPEL)*, 2012, pp. 1–8.

[32] SMA Technologies AG: 'Sunny Island 5048 Installation & Instruction Manual', 2006.

[33] Yang Zhangang, Che Yanbo, and Wang Chengshan, "Construction, operation and control of a laboratory-scale microgrid," in *2009 International Conference on Sustainable Power Generation and Supply*, 2009, pp. 1–5.

[34] J. A. Pec¸as Lopes, C. L. Moreira, and A. G. Madureira, "Defining control strategies for microgrids in islanded operation," *IEEE Trans. Power Syst.*,vol. 21, no. 2, pp. 916–924, 2006.

[35] I. J. Balaguer, Q. Lei, S. Yang, U. Supatti, and Z. Peng, "Control for grid connected and intentional islanding operations of distributed power generation," *IEEE Trans. Ind. Electron*., vol.58, no.1, pp.147,157, Jan. 2011.

Dan Wu received the B.S. degree and M.S. degree in Electrical Engineering from Beijing Institute of Technology, Beijing, China, in 2009 and 2012 respectively. Currently, she is working towards her Ph.D. degree at the department of Energy Technology, Aalborg University, Denmark. She is member of the Microgrid Research Group at Aalborg University. Her areas of interest include microgrids, distributed generation systems.

Fen Tang received the B.S. degree in Electrical Engineering and the Ph.D. degree in Power Electronics & Electric Drives from Beijing Jiaotong University, Beijing, China, in 2006 and 2013, respectively. She is currently a Postdoc in Beijing Jiaotong University. From Jan. 2013 to Jan. 2014 she was a guest Postdoc at Department of Energy Technology, Aalborg University, Denmark.

Her research interests include microgrid, wind power generation system, power converter for renewable generation systems, power quality, and motor control.

Tomislav Dragicevic (S'09-M'13) received the M.E.E. and the Ph.D. degree from the Faculty of Electrical Engineering, Zagreb, Croatia, in 2009 and 2013, respectively. Since 2010, he has been actively cooperating in an industrial project related with design of electrical power supply for remote telecommunication stations. Since 2013 he has been a fulltime Post-Doc at Aalborg University in Denmark. His fields of interest include modeling, control and energy management of intelligent electric vehicle charging stations and other types of microgrids based on renewable energy sources and energy storage technologies.

Juan C. Vasquez (M'12) received the B.S. degree in Electronics Engineering from Autonomous University of Manizales, Colombia in 2004 where he has been teaching courses on digital circuits, servo systems and flexible manufacturing systems. In 2009, He received his Ph.D degree from the Technical University of Catalonia, Barcelona, Spain in 2009 at the Department of Automatic Control Systems and Computer Engineering, from Technical University of Catalonia, Barcelona (Spain), where he worked as Post-doc Assistant and also teaching courses based on renewable energy systems. Since 2011, he has been an Assistant Professor in microgrids at the Institute of Energy Technology, Aalborg University, Aalborg, Denmark, where he is the co-responsible of the microgrids research program. His current research interests include operation, power management, hierarchical control and optimization applied to Distributed Generation in AC/DC microgrids. He is currently member of the Technical Committee on Renewable Energy Systems TC-RES.

Josep M. Guerrero (S'01-M'04-SM'08) received the B.S. degree in telecommunications engineering, the M.S. degree in electronics engineering, and the Ph.D. degree in power electronics from the Technical University of Catalonia, Barcelona, in 1997, 2000 and 2003, respectively. Since 2011, he has been a Full Professor with the Department of Energy Technology, Aalborg University, Denmark, where he is responsible for the Microgrid Research Program. From 2012 he is a guest Professor at the Chinese Academy of Science and the Nanjing University of Aeronautics and Astronautics; and from 2014 he is chair Professor in Shandong University.

His research interests is oriented to different microgrid aspects, including power electronics, distributed energy-storage systems, hierarchical and cooperative control, energy management systems, and optimization of microgrids and islanded minigrids. Prof. Guerrero is an Associate Editor for the IEEE TRANSACTIONS ON POWER ELECTRONICS, the IEEE TRANSACTIONS ON INDUSTRIAL ELECTRONICS, and the IEEE Industrial Electronics Magazine, and an Editor for the IEEE TRANSACTIONS on SMART GRID. He has been Guest Editor of the IEEE TRANSACTIONS ON POWER ELECTRONICS Special Issues: Power Electronics for Wind Energy Conversion and Power Electronics for Microgrids; the IEEE TRANSACTIONS ON INDUSTRIAL ELECTRONICS Special Sections: Uninterruptible Power Supplies systems, Renewable Energy Systems, Distributed Generation and Microgrids, and Industrial Applications and Implementation Issues of the Kalman Filter; and the IEEE TRANSACTIONS on SMART GRID Special Issue on Smart DC Distribution Systems. He was the chair of the Renewable Energy Systems Technical Committee of the IEEE Industrial Electronics Society. In 2014 he was awarded by Thomson Reuters as ISI Highly Cited Researcher.